Available online at www.sciencedirect.com
ScienceDirect
Ceramics International 34 (2008) 1993–2000
CERAMICS INTERNATIONAL
www.elsevier.com/locate/ceramint

Effect of Nb-doping on the microstructure and dielectric properties of $(Ba_{0.80}Sr_{0.20})TiO_3$ ceramics

L. Szymczak *, Z. Ujma, M. Adamczyk, M. Pawełczyk

Institute of Physics, University of Silesia, ul. Uniwersytecka 4, 40-007 Katowice, Poland

Received 17 May 2007; received in revised form 2 June 2007; accepted 21 July 2007
Available online 19 August 2007

Abstract

The effects of cationic substitution of niobium for titanium in $(Ba_{0.80}Sr_{0.20})TiO_3$ composition on the structural and dielectric properties as well as on the electrical conductivity and Seebeck effect were investigated. X-ray diffraction study at room temperature and the real (ε') and imaginary (ε'') parts of permittivity measurements in a wide temperature (from −200 to 450 °C) and frequency (0.1–100 kHz) range were carried out. The analysis of the results of electric conductivity and Seebeck coefficient leads to the conclusion that Nb^{5+} ions, reducing the conductivity of about two orders, are playing role of donors. The correlation between electric characteristics and niobium concentration was confirmed and the evolution from normal ferroelectrics with diffuse phase transition to relaxor ferroelectrics has been found.

Keywords: A. Sintering; B. Electron microscopy; B. X-ray methods; C. Dielectric properties; D. Perovskites

1. Introduction

Lead-free ferroelectric $BaTiO_3$–$SrTiO_3$ solid solutions (BST), intensively studied in recent years [1–8], are of great interest for many practical applications. Due to their outstanding pyroelectric coefficient, large values of the real part of permittivity, low loss tangent and high dielectric breakdown strength, BST ceramics have recently been identified as one of the most promising candidate material for an infrared thermal imaging device called uncooled infrared focal plane arrays [9,10]. In addition, the strong dependence of permittivity on electric field in connection with low dielectric losses makes them attractive for application in tunable microwave devices such as filters, varactors, delay lines and phase shifters, which are essential elements in communication and radar systems [11,12].

Ferroelectric and dielectric properties of BST ceramics strongly depend on the sintering conditions, grain size, porosity, doping amount and structural defects. In our earlier paper [13], the results of the influence of the sintering conditions on the grain structure, phase transitions and dielectric properties of $(Ba_{0.80}Sr_{0.20})TiO_3$ (BST 80/20) ceramics have been reported. It has been shown [13] that an appropriate selection of sintering conditions, and in particular sintering time, leads to the increase of grain size, density of ceramics and to considerable higher values of the real part of permittivity and the remanent polarization. It was also found that an increase of sintering time changes all the parameters describing the phase transitions. These parameters as well as dielectric properties may also be modified by the substitution of selected elements for A or B atoms of the ABO_3 perovskite structure. The strong influence of the heterovalent A site dopants such as Bi^{3+} on the grain structure and electric properties of BST 80/20 ceramics was reported in [14,15].

In the present paper we report the results of experimental study concerning influence of Nb_2O_5 dopant on the grain structure, phase transitions and dielectric properties of BST 80/20 ceramics. It seems that the B site substitutions [16] such as Nb^{5+} [17,18] are more interesting dopants from the fundamental as well as from the technological points of view.

2. Experimental

The BST ceramics of the composition Ba/Sr = 80/20, pure and doped by 0.5–10 mol% Nb_2O_5 were prepared using the conventional mixed-oxide sintering technique. Stoichiometric

* Corresponding author. Tel.: +48 32 2588211x1134; fax: +48 32 2588431.
E-mail address: lidia.szymczak@us.edu.pl (L. Szymczak).

0272-8842/$34.00
doi:10.1016/j.ceramint.2007.07.024

amounts of $BaCO_3$, $SrCO_3$, TiO_2 and Nb_2O_5 oxides were weighed and mixed. The content of Nb_2O_5 was varied from 0 to 10 mol% (i.e. the concentration of Nb in ceramic samples was running from 0 to 20 at%). Thermal synthesis of the pressed mixture was carried out at $T_S = 925$ °C for $t_S = 4$ h. Then the crushed, milled and sieved materials were pressed again into cylindrical pellets and sintered at $T_S = 1250$ °C for $t_S = 4$ h. The latter procedure was repeated before the final sintering, carried out at $T_S = 1460$ °C for $t_S = 7$ h. The Nb additive to the basic composition BST 80/20 improves its sinterability and causes the reduction of porosity. The obtained ceramics with 89–97% theoretical density had good mechanical quality. The bulk density, evaluated by the Archimedes displacement method with distilled water, increased with increasing Nb concentration from 4.90 to 5.92 g/cm^3, for $x = 0.5$ and 10 mol% Nb_2O_5, respectively.

The grain structure and distribution of all the elements throughout the grains was examined by a scanning electron microscope (SEM), JSM-5410 with an energy dispersive X-ray spectrometer (EDS). The grain size measurements were performed on fracture surface of the ceramics. The samples were broken at ambient atmosphere, then covered with gold and placed in the vacuum (10^{-5} Torr) chamber of the electron microscope. The EDS analysis was performed with ISIS-300 SEMQuant program for individual grains of the studied ceramics.

The X-ray diffraction measurements (XRD) were carried out at room temperature on all ceramic samples using Huber diffractometer (Seemann–Bohlin geometry) with monochromatic Cu-Kα_1 radiation (30 kV, 30 mA). The angle scale of received diffraction diagrams was scaled to 2θ (Bragg–Brentano geometry) by Au standard (JCPDS number 12-0403). The diagrams were measured from 20° to 100° in 2θ with 0.05° steps. The calculations were performed using the software for treatment of powder X-ray diffraction data DHN_PDS. In order to receive exact locations, intensities and widths of diffraction lines, the experimental data were fitted to theoretical functions. The attempts of fitting by Gaussian (G), Lorenzian (L), modified Lorenzian (ML) and intermediate Lorenzian (IL) were made. The IL profile showed the best agreement with experimental data and this profile was taken to fit all segments of diagram including diffraction lines. The data received in this manner were used to calculate the unit cell parameters.

The computerized automatic system based on an impedance analyzer HP4192A was used to measure the temperature dependencies of real (ε') and imaginary (ε'') parts of permittivity at several frequencies in the range 0.1–100 kHz of the measuring field. The characteristics $\varepsilon'(T)$ and $\varepsilon''(T)$ were obtained in successive heating–cooling cycles with a constant rate of 2.5 °C/min.

Remanent polarization (P_r) was determined as a function of temperature from the hysteresis loop measurements. Hysteresis loops at 50 Hz and strength 10 kV/cm were examined using the modified Sawyer–Tower method.

Additional measurements of dc electric conductivity and the Seebeck coefficient versus temperature were carried out in the range of 250–450 °C in order to obtain a better explanation of the influence of the Nb dopant on the dielectric characteristics. Weak dc field 10 V/cm was applied to measure the electric conductivity.

All of the ceramic samples were polished before electrical studies to have parallel surfaces and thickness about 0.6 mm, for dielectric and dc conductivity measurements, 0.3 mm for observation of spontaneous polarization, and about 1 mm for the Seebeck coefficient measurements. The samples were coated with silver electrodes using a silver paste without a thermal treatment, and cured at 400 °C for 10 min for deaging prior to measurements. Part of the frozen defects, formed during the sintering process, recombined and the tensions caused by mechanical treatment are partially removed.

3. Results and discussion

3.1. SEM study

The images of microstructure of the BST 80/20 ceramics with Nb_2O_5 content 0.5 and 5 mol% are shown in Fig. 1, as an example. The average grain sizes were 6.2 and 1.6 μm for the ceramics with 0.5 and 5 mol% of Nb_2O_5, respectively. The average grain size of undoped ceramics was larger than 30 μm [13]. The Nb_2O_5 addition produces slightly smaller grains with increasing concentration.

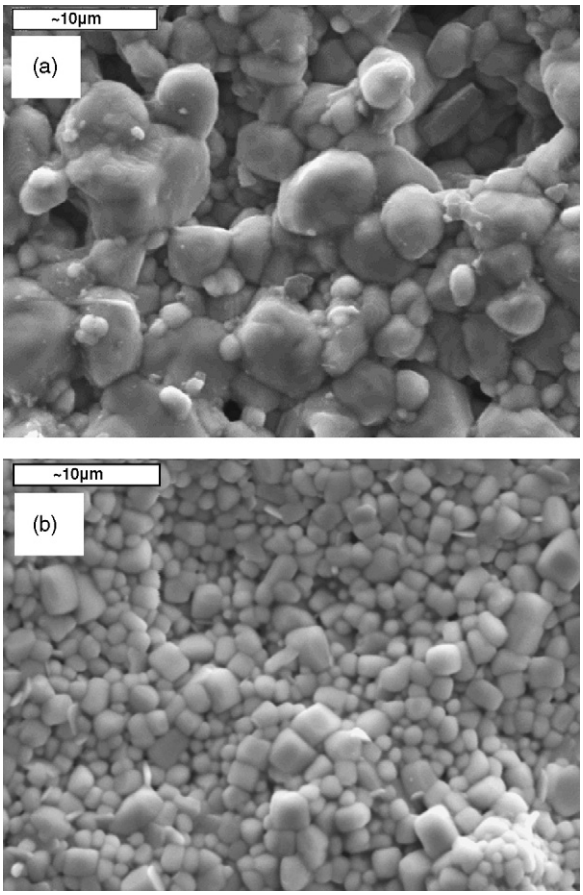

Fig. 1. SEM images of the fracture surface of BST 80/20 + 0.5 mol% Nb_2O_5 (a) and BST 80/20 + 5 mol% Nb_2O_5 (b) ceramics.

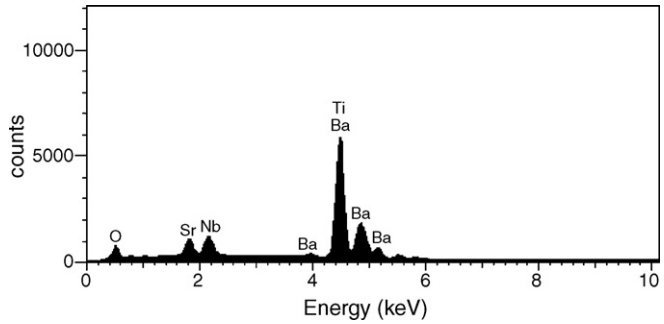

Fig. 2. EDS analysis obtained for one of the grains for BST 80/20 + 5 mol% Nb_2O_5 ceramics.

The EDS analysis, performed for individual grains of the studied ceramics, shows a fairly homogenous distribution of all elements of compound throughout the grains. Moreover, the quantitative microanalysis performed with the implementation of SEMQuant programs elaborated by Oxford Instruments, showed a proper stoichiometry of all samples. The example of EDS analysis, obtained for one of the grains of BST 80/20 + 5 mol% Nb_2O_5 ceramics is shown in Fig. 2.

3.2. X-ray measurements

XRD patterns show that the crystal structures exhibit tetragonal symmetry at room temperature for undoped and containing 0.5–1 mol% Nb_2O_5 BST 80/20 ceramics. When Nb_2O_5 content is larger than 1 mol% the crystal structure exhibits cubic symmetry at room temperature. In all of the studied ceramics a single phase, isostructural perovskite solid solutions, is observed. The example of XRD patterns of undoped BST 80/20 ceramics and with 1 and 10 mol% Nb_2O_5 content obtained at room temperature is shown in Fig. 3.

Unit cell parameters were calculated for all doped BST 80/20 ceramics with what that allowed to determine the average unite cell parameters $\bar{a} = V^{1/3}$ (where V is a unit cell volume). In Fig. 4 a dependence of $\bar{a}$ on Nb_2O_5 concentration is presented. One can notice that the unit cell volume increases with an increase in dopant concentration which seems to

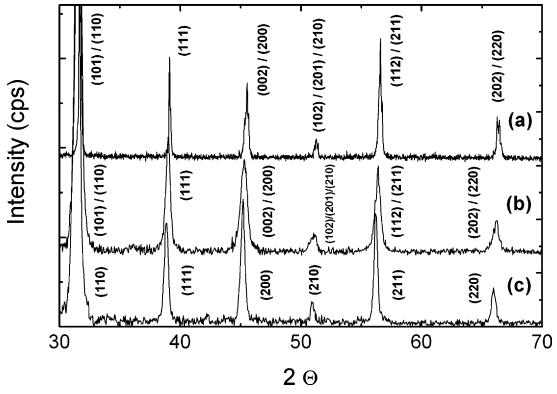

Fig. 3. Parts of the diffraction patterns obtained at the room temperature for undoped BST 80/20 ceramics (a) and doped 1 mol% (b) and 10 mol% (c) Nb_2O_5.

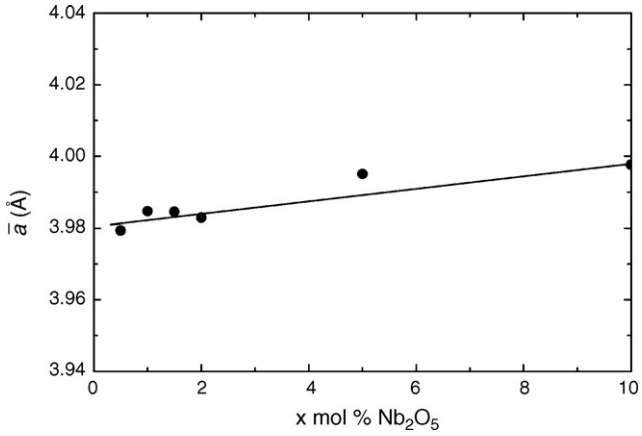

Fig. 4. Average cell parameter versus Nb_2O_5 content for BST 80/20 ceramics.

confirm the supposition that Ti^{4+} ions in solid solutions are substituted by Nb^{5+} ions with larger ionic radius.

An additional confirmation of this supposition may be found in comparison of experimentally determined and theoretically calculated (1 1 1) and (2 0 0) spectral lines intensities. Line intensities were compared for a cubic phase because of the simplicity of calculations. For ceramics with $x = 2$, 5 and 10 mol% of Nb_2O_5 that possessed the regular structure at room temperature, the relative intensities of (2 0 0) and (1 1 1) lines were determined for two possible cases of Nb substitution into the initial compound and namely into an A or B sublattice. The ratios of calculated intensities ($I_{2\,0\,0}/I_{1\,1\,1}$) in dependence on Nb_2O_5 concentration in both cases are presented in Fig. 5. In case of Nb substitution into B sublattice the calculated $I_{2\,0\,0}/I_{1\,1\,1}$ ratio depends on dopant concentration (curve (a) in Fig. 5), whereas in the second case, i.e. when it was considered that Nb ions substitute the A sublattice, the calculated line intensity ratio does not depend on dopant concentration (curve (b) in Fig. 5). The experimentally determined (2 0 0) and (1 1 1) lines intensity ratio depends on Nb concentration (curve (c) in Fig. 5) and therefore confirms the first model.

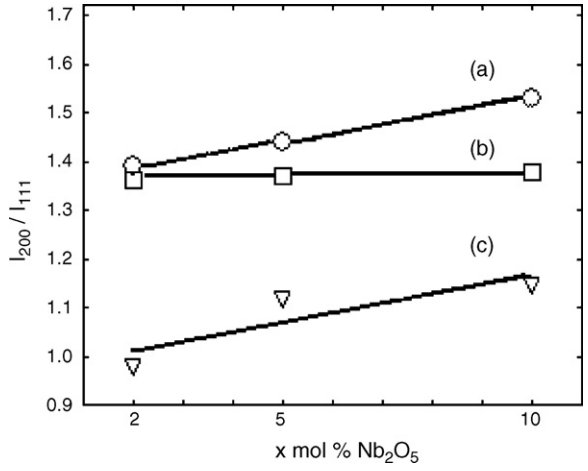

Fig. 5. Calculated (a and b) and experimentally obtained (c) spectral lines intensity ratio for BST 80/20 + x mol% Nb_2O_5 ceramics.

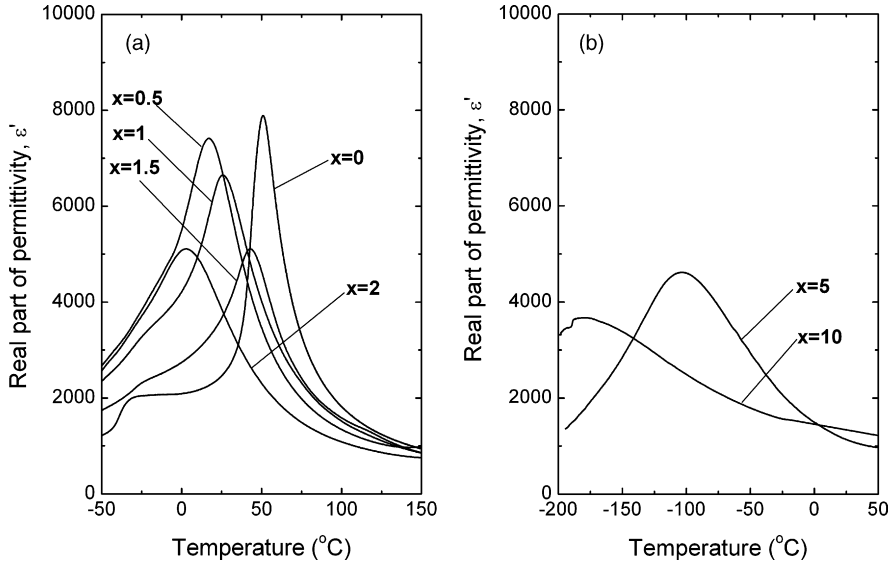

Fig. 6. Real part of permittivity as a function of temperature measured on heating at frequency of measuring field 1 kHz for BST 80/20 ceramics with various Nb_2O_5 content.

3.3. Dielectric properties and phase diagram

The comparison of the $\varepsilon'(T)$ curves, measured on heating at frequency 1 kHz, for undoped and Nb-modified BST 80/20 ceramics is shown in Fig. 6. It can be seen that for Nb_2O_5 content smaller than 2 mol%, the $\varepsilon'(T)$ curves reveal anomalies in the vicinity of temperatures corresponding to the orthorhombic–tetragonal (F_O–F_T) and tetragonal–cubic (F_T–P_C) phase transitions (Fig. 6(a)). An anomaly in the vicinity of temperatures corresponding to the rhombohedral–orthorhombic (F_R–F_O) phase transition, for ceramics with 1.5 and 2 mol% Nb_2O_5, is visible only in $d\varepsilon'/dT(T)$ dependences. The temperature intervals between the three phase transitions become narrower when Nb concentration increases. The three anomalies in $\varepsilon'(T)$ curves associated with the structural phase transitions eventually merge into a broad peak for the largest niobium concentrations, i.e. 5 and 10 mol% (Fig. 6(b)). Based on the dielectric measurements, a phase diagram of BST 80/20 + x mol% Nb_2O_5 ceramics was plotted (Fig. 7). The $T_{F_R-F_O}$ phase transition temperature for undoped BST 80/20 ceramics shown in this figure is quoted according to [6].

The dielectric response shows a strongly diffused character of the ferroelectric–paraelectric phase transition (DPT) for all investigated ceramics. Fig. 8 depicts the reciprocal ε' versus temperature for the BST 80/20 + x mol% Nb_2O_5 ceramics. It can be seen that the Curie–Weiss law, $1/\varepsilon' = C/(T - T_o)$ (where C is the Curie–Weiss constant and T_o is the Curie–Weiss temperature), is observed in the paraelectric phase only at temperatures much higher than T_m corresponding to broadened maximum in the $\varepsilon'(T)$ curves, i.e. above T_{C-W} temperature. In the temperature range between T_m and T_{C-W} the temperature dependence of real part of permittivity obeys the empirical expression which describes DPT as follows:

$$\frac{1}{\varepsilon'} - \frac{1}{\varepsilon'_{max}} = C'(T - T_m)^{\gamma} \quad (1)$$

where γ is the diffuseness exponent and $1 \leq \gamma \leq 2$. The determined parameter γ versus Nb content is shown in Fig. 9. It can be noted that the value of exponent γ depends strongly on the Nb_2O_5 content. Other characteristic parameters determined and calculated from 100 kHz dielectric response for undoped and Nb-doped BST 80/20 ceramics are listed in Table 1.

The temperature dependencies of the real part of permittivity at various frequencies in the range 0.1–100 kHz of the measuring field for the undoped and Nb-doped ceramics show two kinds of dispersion. The first is connected with the diffuse phase transition occurring in the range of T_m. Both T_m and ε'_{max}

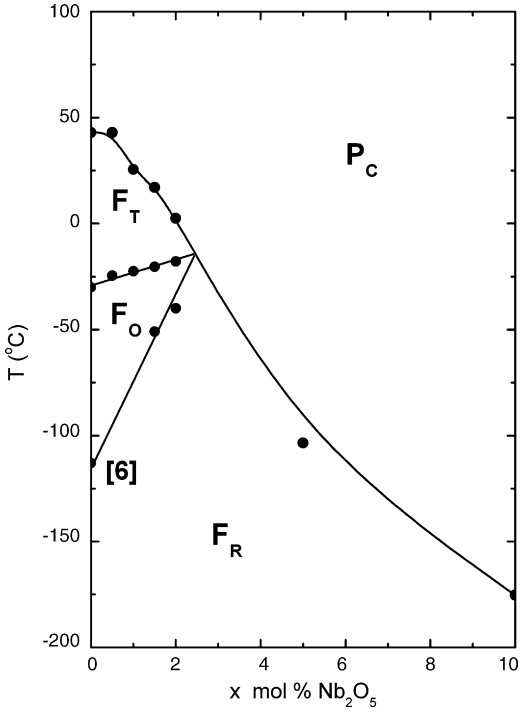

Fig. 7. Variations of phase transition temperatures versus Nb_2O_5 content.

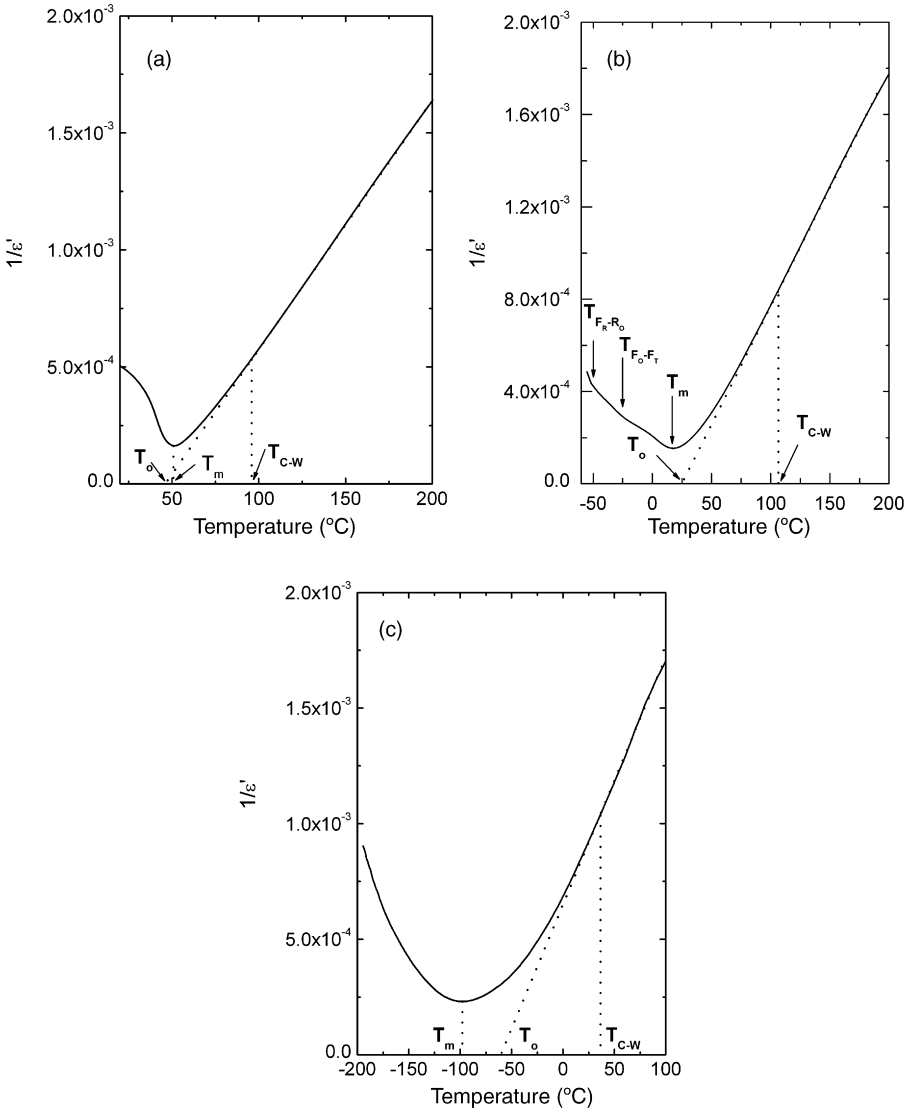

Fig. 8. Inverse of the 100 kHz real part of permittivity versus temperature for undoped BST 80/20 ceramics (a) and doped 1.5 mol% (b) and 5 mol% (c) Nb_2O_5.

depend on the frequency of the measuring field. This fact is more distinct for Nb-modified ceramics. The degree of frequency dispersion can be described by the value of $\Delta\varepsilon'_{max}$ defined as the difference between the ε'_{max} measured at 0.1 kHz and that measured at 100 kHz, and ΔT_m, defined in the similar manner (Fig. 10). It is noteworthy that the value of ΔT_m increases strongly from 0.5 °C for the undoped to 8 and 10 °C for 5 and 10 mol% Nb_2O_5-modified BST 80/20 ceramics, respectively.

For highly Nb-modified (5 and 10 mol%) BST 80/20 ceramics, the $\varepsilon'(f)$ and $\varepsilon''(f)$ characteristics exhibit behavior typical for ferroelectric relaxors (Fig. 11) [19,20]. The relaxor characteristics can be explained in terms of the breakdown of long-range ferroelectric interactions by defects and/or impurities, thus preventing the evolution of the normal long-range ferroelectric order and favoring the formation of a state with short-range polar ordering. Randomly distributed charged defects and/or defect clusters create random electric fields on atomic length scales [21]. These random fields suppress the ferroelectricity of BST solid solutions, resulting in the relaxor behavior of Nb-doped BST ceramics.

The second kind of dispersion occurs at temperatures higher than 200 °C, i.e. in the paraelectric phase. It is more visible for lower frequency and gradually disappears when the frequency excesses 10 kHz. Such behavior was found for many ferroelectrics with the perovskite-type structure [22,23], as well as for undoped BST 80/20 ceramics [13]. The insertion of the Nb dopant to ceramics caused gradual decay of this dispersion in the region of the paraelectric phase.

The temperature dependencies of the remanent polarization (P_r) obtained on heating for BST 80/20 ceramics with various Nb_2O_5 contents, are shown in Fig. 12. The course of the $P_r(T)$ curves differs significantly from those observed in the vicinity of the normal ferroelectric phase transition, particularly in a wide temperature range in the neighborhood of T_m, corresponding to the maxima in $\varepsilon'(T)$ curves (ferroelectric–paraelectric phase transition) (Fig. 12). In the case of undoped BST ceramics the maximum value of P_r is small ($P_r \approx 8$ μC/

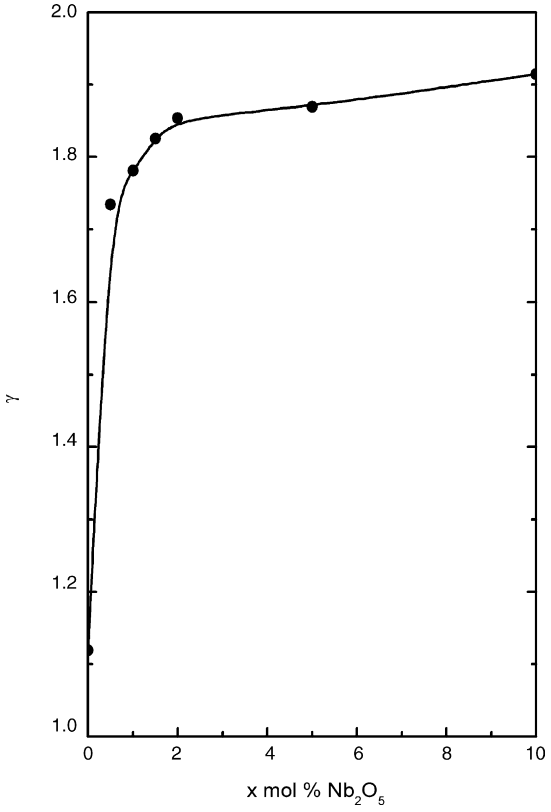

Fig. 9. Diffuseness exponent γ versus Nb_2O_5 content.

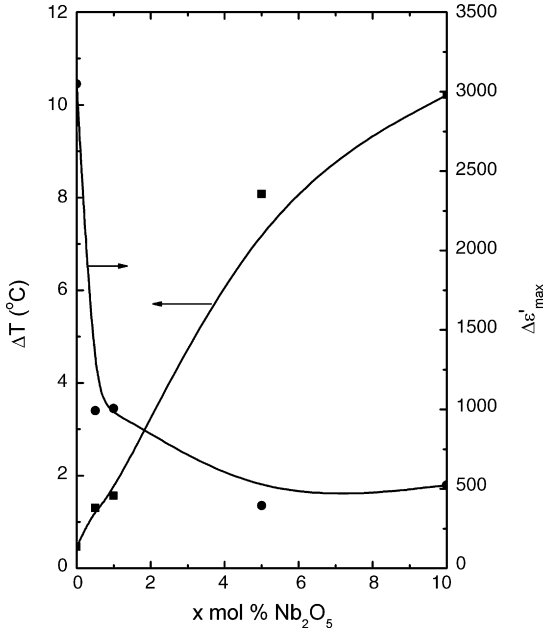

Fig. 10. Degree of frequency dispersion of $\Delta T_m = T_m$ (100 kHz)–T_m (0.1 kHz) and $\Delta\varepsilon'_{max} = \varepsilon'_{max}$ (0.1 kHz)–ε'_{max} (100 kHz) as a function of Nb_2O_5 content.

cm^2) at room temperature and gradually decreases with niobium concentration to ca. 4 μC/cm^2 for $x = 2$ mol% Nb_2O_5.

3.4. Electric conductivity and Seebeck coefficient

The influence of the substitution of Nb^{5+} for Ti^{4+} sublattice on the balance of electron–hole carriers was studied using the measurements of dc electric conductivity (σ) and the Seebeck coefficient (α) in the wide range of paraelectric phase (200–450 °C). In order to establish the type of electric conductivity, thermoelectric studies were carried out and the Seebeck coefficient was determined. The experimental technique employed was described in our earlier paper [24]. The results of measurements of the dc conductivity and the Seebeck coefficient as a function of Nb_2O_5 obtained at $T = 400$ °C are shown as example in Fig. 13.

The addition of Nb_2O_5 to BST 80/20 ceramics and the substitution of Nb^{5+} ions for Ti^{4+} ions causes a change of the values of electric conductivity and its character from the p-type into n-type. This should be accompanied by the effect of an increase of A^{2+} position vacancy concentration in ABO_3

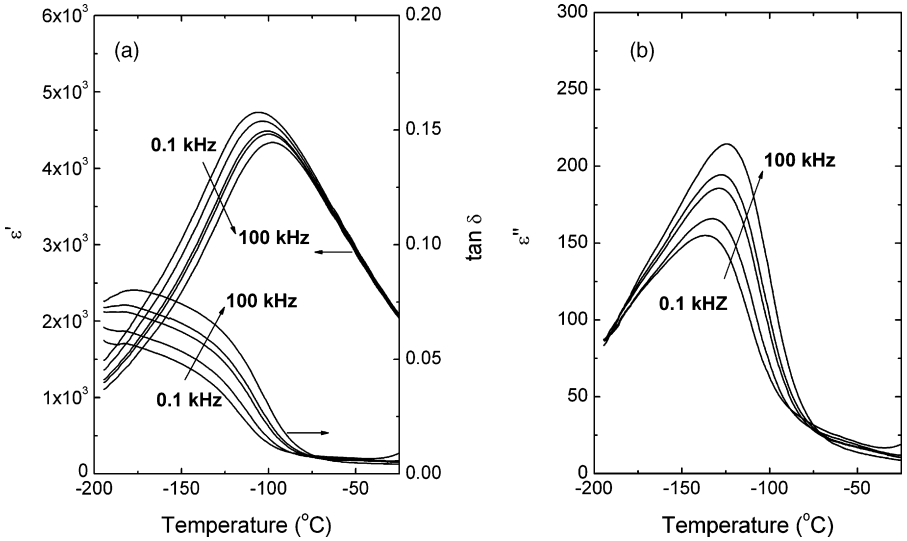

Fig. 11. Real (a) and imaginary (b) parts of permittivity as a function of temperature measured at various frequencies of measuring field for BST 80/20 + 5 mol% Nb_2O_5 ceramics. The loss factor versus temperature is also shown in (a). The individual curves concern frequencies: 0.1, 1, 10, 20 and 100 kHz.

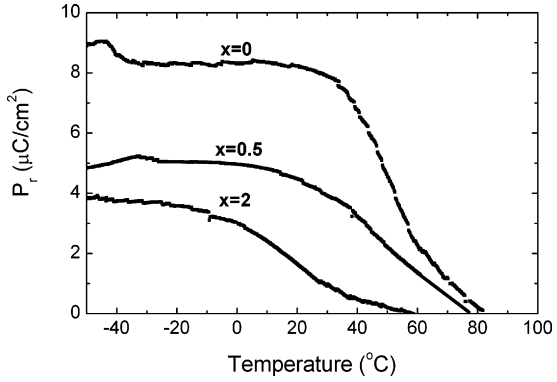

Fig. 12. Remanent polarization versus temperature determined on heating from hysteresis loop measurements at field of 10 kV/cm for BST 80/20 ceramics with various Nb_2O_5 content.

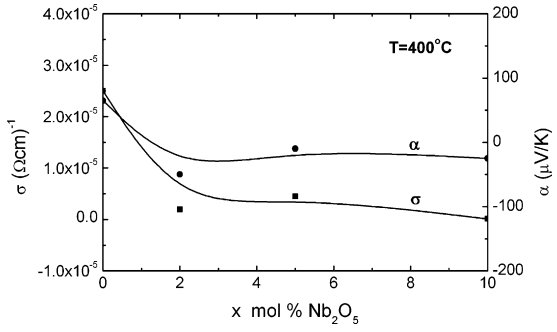

Fig. 13. Seebeck coefficient (α) and electric conductivity (σ) obtained at 400 °C versus Nb_2O_5 content.

perovskite structure. The presence of A^{2+} and O^{2-} vacancies exerts a strong influence on the balance of the charge carriers transport process. Undoped ceramics exhibit p-type of electric conductivity which is caused by predomination of A^{2+} vacancies acting as acceptor centres. Analysis of the results of electric conductivity and Seebeck coefficient studies presented above also leads to the conclusion that Nb^{5+} ions substitution for Ti^{4+} plays part of donors in the investigated samples. This leads to decrease of conductivity of about two orders of magnitude, comparing to undoped BST ceramics, due to the compensation of already existing holes by electrons from donor dopant, with simultaneous change in type of electric conductivity from p-type to n-type.

Table 1
Characteristic parameters determined and calculated from $\varepsilon'(T)$ measurements at 100 kHz for undoped ($x = 0$) and Nb_2O_5-modified ($x = 0.5$–10) BST 80/20 ceramics

x (mol%)	T_m (°C)	T_o (°C)	T_{C-W} (°C)	$C \times 10^5$ (°C)
0	48.14	46.20	96.90	1.06
0.5	43.5	61.82	119.7	1.32
1	26.24	41.30	115.5	1.07
1.5	17.7	23.04	106.3	1.01
2	3.4	11.50	100.1	1.16
5	−97.7	−57.84	36.5	1.10
10	−169.5	−155.5	−44.85	0.67

4. Conclusions

The obtained experimental data show that Nb dopant strongly modify the sinterability, grain structure, temperatures of phase transitions and all the investigated characteristics of BST 80/20 ceramics. The increase of the Nb concentration leads to the decrease of grain size, the increase of density and the improvement of the quality of the investigated ceramics. The temperature intervals between the three consecutive ferroelectric transitions become narrower as Nb^{5+} ions are substituted for Ti^{4+} ions in the B-site sublattice of BST 80/20 ceramics and as the results of this, three peaks associated with the structural phase transitions coalesce, exhibiting a broad dielectric response for Nb_2O_5 content higher than 2 mol%. Moreover, highly Nb-modified ($x = 5$ and 10 mol%) ceramics exhibit the features of ferroelectric relaxors, i.e. the ε'_{max} significantly decreases and the T_m shifts towards higher temperatures with an increase in frequency of measuring field. Additional anomalies in $\varepsilon'(T)$ curves in the low frequency range, present in the paraelectric phase for the undoped ceramics, are eliminated by the Nb dopant which also reduces the dc conductivity by about two orders of magnitude.

References

[1] H. Kobayashi, T. Kobayashi, Heteroepitaxial growth of quaternary $Ba_xSr_{1-x}TiO_3$ thin films by ArF excimer laser ablation, Jpn. J. Appl. Phys. 33 (1994) 533–536.
[2] C.S. Chern, C.S. Chern, S. Liang, Z.Q. Shi, S. Yoon, A. Safari, P. Lu, B.H. Kear, B.H. Goodreau, T.J. Marks, S.Y. Hou, Heteroepitaxial growth of $Ba_{1-x}Sr_xTiO_3/YBa_2Cu_3O_{7-x}$ by plasma-enhanced metalorganic chemical vapor deposition, Appl. Phys. Lett. 64 (1994) 3181–3183.
[3] I. Suzuki, M. Eijima, K. Watanabe, Y.-M. Xiong, T. Saitohu, Spectroscopic ellipsometry characterization of $Ba_{0.70}Sr_{0.30}TiO_3$ thin films prepared by the sol–gel method, Thin Solid Films 313–314 (1998) 214–217.
[4] T. Ota, M. Tani, Y. Hikichi, H. Unuma, M. Takahashi, H. Suzuki, Dielectric property of $BaTiO_3$-based ceramics with gradient compositions, Ceram. Trans. 100 (1999) 51–60.
[5] U. Syamaprasad, R.K. Galgali, B.C. Mohanty, Dielectric properties of the $Ba_{1-x}Sr_xTiO_3$ system, Mater. Lett. 7 (1988) 197–200.
[6] V.V. Lemanov, E.P. Smirnova, P.P. Syrnikov, E.A. Tarakanov, Phase transitions and glasslike behaviour in $Sr_{1-x}Ba_xTiO_3$, Phys. Rev. B 54 (1996) 3151–3157.
[7] R. Wang, Y. Inaguma, M. Itoh, Dielectric properties and phase transition mechanisms in $Sr_{1-x}Ba_xTiO_3$ solid solution at low doping concentration, Mater. Res. Bull. 36 (2001) 1693–1701.
[8] V.S. Tiwari, N. Singh, D. Pandey, Diffuse ferroelectric transition and relaxational dipolar freezing in $(Ba,Sr)TiO_3$, J. Phys. Condens. Matter 7 (1995) 1441–1460.
[9] S. Liu, M. Liu, Y. Zeng, Y. Huang, Preparation phase transition diffuseness and ferroelectric fatigue behavior of $Ba_{0.85}Sr_{0.15}TiO_3$ thin film for uncooled infrared focal plane arrays, Mater. Sci. Eng. B 90 (2002) 149–153.
[10] R. Watton, M.A. Todd, Induced pyroelectricity in sputtered lead scandium tantalate films and their merit for IR detector arrays, Ferroelectrics 118 (1991) 279–295.
[11] F. Zimmermann, M. Voights, C. Weil, R. Jakoby, P. Wang, W. Menesklou, E. Ivers-Tiffe, Investigation of barium strontium titanate thick films for tunable phase shifters, J. Eur. Ceram. Soc. 21 (2001) 2019–2023.

[12] S.-G. Lee, C.-I. Kim, J.-P. Kim, S.-H. Lee, Structural and dielectric properties of barium strontium calcium titanate thick films modified with MnO_2 for phased array antennas, Mater. Lett. 58 (2003) 110–114.

[13] L. Szymczak, Z. Ujma, J. Hańderek, J. Kapusta, Sintering effects on dielectric properties of (Ba,Sr)TiO_3 ceramics, Ceram. Int. 30 (2004) 1003–1008.

[14] L. Szymczak, L. Kozielski, M. Adamczyk, A. Lisińska-Czekaj, Z. Ujma, D. Czekaj, Dielectric, pyroelectric and thermally stimulated depolarization current investigations on (Ba,Sr)TiO_3 ceramics with Bi_2O_3 additive, Ferroelectrics 349 (2007) 179–189.

[15] L. Zhou, P.M. Vilarinho, J.L. Baptista, Dielectric properties of bismuth doped $Ba_{1-x}Sr_xTiO_3$ ceramics, J. Eur. Ceram. Soc. 21 (2001) 531–534.

[16] R. Farhi, M.El. Marssa, A. Simon, J. Ravez, Relaxor-like and spectroscopic properties of niobium modified barium titanate, Eur. Phys. J. B 18 (2000) 605–610.

[17] S. Garcia, R. Font, J. Portelles, R.J. Quinones, J. Heiras, J.M. Siqueiros, Effect of Nb doping on (Sr,Ba)TiO_3 ceramic samples, J. Electroceram. 6 (2001) 101–108.

[18] Z.H. Zhou, P. Du, W. Wen, G. Han, G. Shen, Dielectric properties of $0.7BaO{\cdot}0.3SrO{\cdot}(1-y)TiO_2{\cdot}yNb_2O_5$ composite ceramics, Mater. Chem. Phys. 87 (2004) 430–434.

[19] Z.Y. Cheng, X. Yao, A. Guo, Model study of contribution of polar-regions to dielectric property for relaxor ferroelectrics, Ferroelectrics 190 (1997) 167.

[20] M. Adamczyk, Z. Ujma, L. Szymczak, I. Gruszka, Effect of Nb doping on the relaxor behaviour of $(Pb_{0.75}Ba_{0.25})(Zr_{0.70}Ti_{0.30})O_3$ ceramics, J. Eur. Ceram. Soc. 26 (2006) 331–336.

[21] W. Kleemann, Random-field-induced antiferromagnetic, ferroelectric, and structural domain states, Int. J. Mod. Phys. B 7 (1993) 2469.

[22] Z. Ujma, L. Szymczak, J. Hańderek, K. Szot, H.J. Penkalla, Dielectric and pyroelectric properties of Nb-doped $Pb(Zr_{0.92}Ti_{0.08})O_3$ ceramics, J. Eur. Ceram. Soc. 20 (2000) 1003–1010.

[23] M. Maglione, Dielectric relaxation and conductivity in ferroelectric perovskites, Ferroelectrics 176 (1996) 1–6.

[24] J. Hańderek, Z. Wróbel, K. Wójcik, Z. Ujma, Specific problems of thermoelectric force investigations in lead titanate, potassium niobate, and sodium niobate single crystals and in lead zirconate ceramics, Ferroelectrics 17 (1977) 60.